Neurobiology of Disease 205 (2025) 106781

Contents lists available at ScienceDirect

Neurobiology of Disease

journal homepage: www.elsevier.com/locate/ynbdi

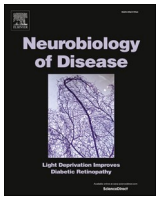

Haploinsufficiency of PDE2A causes in mice increased exploratory behavior associated with upregulation of neural nitric oxide synthase in the striatum

Ana Gabriela de Oliveira do Rêgo [a,1], Francesca D'Amico [a,1], Vincenza D'Angelo [b], Silvia Cardarelli [a], Debora Cutuli [c,d], Davide Decandia [c,d], Eugenia Landolfo [c], Laura Petrosini [c], Manuela Pellegrini [e], Marcello D'Amelio [c,f], Nicola Biagio Mercuri [b,c], Mauro Giorgi [a,*], Giuseppe Sancesario [b]

[a] Department of Biology and Biotechnology "Charles Darwin", Sapienza University, 00185 Rome, Italy
[b] Department of Systems Medicine, Tor Vergata University, 00133 Rome, Italy
[c] IRCCS Santa Lucia Foundation, 00179 Rome, Italy
[d] Department of Psychology, Sapienza University, 00185 Rome, Italy
[e] Institute of Biochemistry and Cell Biology, IBBC-CNR, 00015 Monterotondo Scalo, Rome, Italy
[f] Department of Medicine, Campus Biomedico University, 00128 Rome, Italy

ARTICLE INFO

Keywords:
Phosphodiesterase 2A
PDE2A heterozygous +/− mice
cAMP
cGMP
PDE3
PDE5
PDE9
PDE10
nNOS
Exploratory behavior

ABSTRACT

Phosphodiesterase 2 A (PDE2A) function is stimulated by cGMP to catabolize cAMP. However, neurological and neurochemical effects of PDE2A deficiency are poorly understood. To address this gap, we studied behavioral characteristics and cerebral morpho-chemical changes of adult male heterozygous C57BL/6-PDE2A+/− (HET), and wild type C57BL/6-PDE2A+/+ (WT) mice.

Behavioral functions of mice were evaluated by a wide test battery. HET mice exhibited greater tendency to explore novel environments in comparison to WT mice, but spatial working memory, anxiety, and sociability were similar in adult HET and WT mice.

In HET mice, PDE2A mRNA, PDE2A protein expression, and cGMP hydrolyzing enzymatic activity were consistently reduced by about 50 %. Consequently, the cyclic nucleotide levels were significantly increased in HET mice, but unexpectedly the mean percentage variation was higher for cGMP equal to 153.23 %, and lower for cAMP equal to 16.41 %. Therefore, to try to explain the preponderant increase of cGMP to cAMP we evaluated other PDE enzymes functionally related to PDE2A. Surprisingly, results were quite contradictory: in HET mice protein levels of the other dual-specificity enzyme PDE3A and PDE10A were reduced, whereas the expressions of PDE5A and PDE9A that selectively hydrolyze cGMP were increased.

Therefore, we investigated the involvement of neuronal nitric oxide synthase (nNOS) expression, as determinant of a possible increased synthesis of NO/cGMP signaling. Interestingly, in HET mice the expression level of brain nNOS, measured by western blot and immune-histochemistry was significantly increased, particularly in interneurons from the striatum.

In conclusion, the deficiency of PDE2A could be compensated in the striatum by upregulating nNOS/NO/cGMP pathway, which in turn likely upregulates PDE2A-dependent cAMP hydrolysis. The neuroanatomical correlation between striatal nNOS upregulation and the behavioral phenotype of increased exploratory behavior in HET mice is advanced.

1. Introduction

Second messenger 3′,5′-cyclic adenosine monophosphate (cAMP) and 3′,5′-cyclic guanosine monophosphate (cGMP) play important roles in transduction of a signal from outside the cell to the appropriate molecules within the cell. These second messengers bind to cyclic

* Corresponding author.
E-mail address: mauro.giorgi@uniroma1.it (M. Giorgi).
[1] These authors to be considered equally first author.

https://doi.org/10.1016/j.nbd.2024.106781
Received 30 July 2024; Received in revised form 21 December 2024; Accepted 21 December 2024
Available online 27 December 2024

nucleotide-gated ion channels and to target proteins like protein kinases, namely, protein kinase A and G (Podda and Grassi, 2014).

cAMP and cGMP are synthesized by adenylyl cyclase or guanylate cyclase, respectively, and degraded by cyclic nucleotide phosphodiesterase (PDE) superfamily of enzymes, encompassing a total of 11 different types of PDEs (PDE1–PDE11). PDEs have individual and distinct degrees of substrate specificity. The cAMP-specific PDEs include PDE4, PDE7, and PDE8; the cGMP-specific enzymes include PDE5, PDE6, and PDE9; the remaining family members process both cyclic nucleotides, although they prefer one or the other to varying degrees (Francis et al., 2011).

Namely, PDE2A catabolizes both cAMP and cGMP, and allosteric binding cGMP increases its hydrolytic activity of cAMP by ~5–6 times (Sadek et al., 2020). PDE2A is involved in regulating many intracellular processes, corresponding to its tissue-specific expression. Indeed, PDE2A is widely distributed in a number of organs including the brain, where it is most abundant in the limbic system, frontal cortex, and striatum, regions known to be involved in cognitive, emotional and motor functions. PDE2A is the only PDE associated with docked synaptic vesicles, resulting thus involved in presynaptic plasticity (Boyken et al., 2013). Recently, it has been demonstrated that about 50 % of the total amount of hydrolyzed cGMP is PDE2A-dependent during rat brain synaptogenesis, a further significative index of the key role of PDE2A in brain development (Maurin et al., 2019).

Moreover, PDE2A has received considerable interest after the discovery that its increased expression and activity in the brain are a molecular determinant in the physiopathology of the fragile X syndrome, the most common monogenic cause of autism (Maurin et al., 2019). Consistently, patients affected by Autism Spectrum Disorders (ASD) with moderate to severe intellectual disability display homozygous mutations in PDE2A (Doummar et al., 2020; Haidar et al., 2020; Salpietro et al., 2018; Yousaf et al., 2023). On the other hand, reduced PDE2A levels in amygdala and frontal cortex have been found in *post-mortem* analyses of patients with schizophrenia (Farmer et al., 2020). Moreover, the pharmacological inhibition of PDE2A in genetic and environmental preclinical models of ASD rescues the dendritic spines maturity and the exaggerated hippocampal long-term depression (LTD), as well as the social and communicative deficits. These preclinical results suggest that PDE2A blockade may represent a reliable therapeutic approach to treat neurochemical changes and social deficits common to ASD (Schiavi et al., 2022).

A clear indication of the importance of PDE2A during development derives from the observation that its genetic ablation lethally impairs heart and liver development in mouse embryos, leading to death after the second week of fetal development (Assenza et al., 2018; Barbagallo et al., 2020; Cardarelli et al., 2024). While knockout PDE2A−/− embryos do not survive, heterozygous PDE2A+/− mice have apparent normal development, and standard life expectancy. However, a recent study (Delhaye et al., 2024) characterized the pup and adolescent PDE2A heterozygous +/− mice at behavioral, cellular, molecular and electrophysiological levels, revealing some changes in molecular targets of the PDE2A-dependent pathway, underlying subtle socio-cognitive deficits, and proposing the PDE2A heterozygous +/− mice as a developmental brain disorder model. The socio-cognitive deficits were associated with microglia activation, and defects in AMPA receptor trafficking (Delhaye et al., 2024).

Considering that the deficiency of PDE2A activity appears to be involved in subtle socio-cognitive deficits in infancy and adolescence, we retained interesting to analyze further whether such deficits remain or further develop in the mature age. Therefore, we evaluated the behavior of adult heterozygous PDE2A +/− mice, considering in particular spatial working memory, explorativity, sociability, and anxious and depressive-like behaviors. Moreover, we evaluated eventual compensatory changes to PDE2A deficiency, able to modulate cAMP and cGMP homeostasis, considering the functionality of other PDE enzymes related to PDE2A functions (PDE3A, PDE10A and PDE5A, PDE9A); finally, we evaluated possible changes of cGMP synthesis, related to nNOS/NO pathway, to increase the PDE2A hydrolytic activity of cAMP.

2. Materials and methods

2.1. Animals

Wild type PDE2A+/+ mice (C57Bl/6 J) and PDE2A+/− mice (B6; 129P2 - Pde2a < tm1Dgen>/H; EM: 02366) were obtained from EMMA (UK). Genotyping for PDE2A was performed as previously reported (Assenza et al., 2018). Mice were kept under artificial day-night cycle, with free access to food and water. All experimental procedures were conforming with the Directive 2010/63/EU of the European Parliament on the protection of animals used for scientific purposes and were conducted with the approval of the Italian Ministry of Health 919/2020-PR dated 28/09/2020.

2.2. Behavioral testing and experimental procedures

Male adult PDE2A +/− heterozygous (HET) and PDE2A +/+ wild type (WT) mice, with similar body weight (30–32 g) at the adult age of 3–4 months, were tested with the following validated behavioral tasks, tapping distinct cognitive functions: Open Field (OF) to assess exploratory behavior and anxiety levels; Marble Burying Test (MBT) to assess neophobic, anxious, and compulsive behaviors; Elevated Plus Maze (EPM) to evaluate anxiety levels; Light/Dark Box Test (L/D) to assess neophobic and anxious behavior; Tail Suspension Test (TST) to measure depressive-like behaviors; Y-Maze Spontaneous Alternation Test (Y-Maze) to measure spatial working memory and willingness of mice to explore new environments; Three-Chamber Sociability Test (ST) to assess general sociability (for the description of behavioral tasks, see Supplementary Materials). At the end of behavioral testing, the animals were sacrificed under deep anesthesia and the brains were used for morphological and biochemical analyses.

2.3. Morphological and biochemical analyses

For morphological studies, animals were deeply anesthetized and transcardially perfused with 4 % paraformaldehyde. Brains were immediately removed and postfixed in the 4 % paraformaldehyde fixative solution overnight at 4 °C. Using an Oxford vibratome, 40 μm thick coronal brain sections were cut across the entire rostro-caudal extent, collected, and stored at 4 °C, as previously reported (D'Angelo et al., 2017).

For biochemical analyses, animals were killed by cervical dislocation, and their brains were rapidly removed and placed on an ice-cold plate. Thick brain sections were cut with an Oxford vibratome, promptly frozen in liquid nitrogen, and stored at −80 °C. Selected brain regions were homogenized using a glass homogenizer: the first and second supernatants were then pooled and processed for biochemical analysis, as previously reported (Giorgi et al., 2008).

2.4. Western blotting

Protein samples were extracted from adult brains in RIPA lysis buffer 1× (Merck Millipore Darmstadt, Germany) supplemented with protease and phosphatase inhibitors. The protein concentration was measured by Bradford method. An amount of 30 μg of protein was electrophoresed in 8 % SDS-PAGE gels and transferred onto nitrocellulose membrane (Bio-Rad). Blots were incubated overnight at 4 °C either with anti-PDE2A antibody (1:1000; Abcam, #ab140650), or anti-PDE3A antibody (1:500; Santa Cruz, #sc-20,792), or anti-PDE5A antibody (1:1000; Santa Cruz #32884), or PDE9A (1:1000; Abcam, #ab125672), or PDE10A antibody (1:500; FabGennix, #PD10A-101AP), or anti-nNOS (1:500; Sigma-Aldrich, # 07–571-I). Anti- GAPDH antibody (1:10000; Sigma-Aldrich, #G9545) or anti-β-actin antibody (1:10000; Sigma-Aldrich,

#A1978) were used as housekeeping proteins.

After, the membranes were incubated in appropriated horseradish peroxidase (HRP)-conjugated secondary antibodies for 1 h at room temperature, and signals were detected by chemiluminescence with the ECL SuperSignal TM West Pico PLUS substrate (Thermo Fisher Scientific, MA, USA). Chemiluminescent images of immunodetected bands were recorded with the Syngene G-box system (Syngene Bioimaging, India) and the densitometric analysis was performed using the National Institutes of Health ImageJ version l.29 program.

2.5. RNA preparation and RT-qPCR

Total RNA was isolated from tissue samples using the RNA purification kit from Zymo Research (CA, USA), according to the manufacture's protocol. The yield and purity of RNA was determined with the NanoDropTM OneC microvolume UV–Vis Spectrophotometer (Thermo Fisher Scientific, MA, USA). The RNA was reverse-transcribed to synthesize cDNA through Maxima H minus reverse transcriptase (Thermo Fischer Scientific, Waltham, MA, USA), according to the manufacturer's protocol. qPCR was performed on reverse-transcription (RT) products with the PowerUp SYBR Green Master Mix (Thermo Fisher Scientific, MA, USA) and the following specific primers: *Pde2a-For* 5'-ACCGAAAGATCCTGCAACTG-3′, *Pde2a-Rev* 5'-TTCTCCCAGCACTTTGTCTC-3′; *Gapdh-For* 5'-GTGAAGGTCGGTGTGAACG-3′, *Gapdh-Rev* 5'-ATTTGATGTTAGTGGGGTCTCG-3′.

Target transcripts were analyzed using QuantStudio 7 Flex RT PCR System (Thermo Fisher Scientific, MA, USA). For quantification analysis, the comparative threshold cycle (Ct) method was used. The Ct value of *Pde2a* gene was normalized to the Ct value of *Gapdh* in the same cDNA sample. The gene expression levels were evaluated by the fold change using the eq. $2^{-\Delta\Delta Ct}$.

2.6. PDE2A activity assay

Brains were homogenized using a glass homogenizer in 20 mM Tris-HCl buffer pH 7.2 containing 0.2 mM EGTA, 5 mM β-mercaptoethanol, 2 % (*v*/v) antiprotease cocktail (Merck KGaA, Germany), 1 mM PMSF, 5 mM $MgCl_2$, 0.1 % (v/v) Triton X-100. The homogenates were centrifuged at 14,000 ×*g* for 30 min at +4 °C. Phosphodiesterase activity was measured on the supernatant with the method described by Thompson and Appleman (Thompson and Appleman, 1971) in 60 mM Hepes pH 7.2, 0.1 mM EGTA, 5 mM $MgCl_2$, 0.5 mg/mL bovine serum albumin and 30 mg/mL soybean trypsin inhibitor in a final volume of 0.15 mL. The reaction was started by adding tritiated substrates at a final concentration of 1 μM [^{3}H]cGMP. The reaction was stopped by adding 50 μl of 0.1 N HCl and then neutralized with 50 μl of 0.1 N NaOH in 0.1 M Tris-HCl pH 8.0. Subsequently, 25 μl of 2 mg/ml of 5′-nucleotidase (snake venom from *Crotalus atrox*; Merck KGaA) in 0.1 M Tris-HCl pH 8.0 were added. Samples were gently mixed and incubated at 30 °C for 30 min to allow complete conversion of 5′-nucleotide to its corresponding nucleoside. Unhydrolyzed cyclic nucleotide and the corresponding nucleoside were separated by DEAE Sephadex A-25 columns. The eluate was mixed with ULTIMA GOLD scintillation liquid (PerkinElmer, USA) and counted on a Tri-Carb 2100TR Liquid Scintillation Counter (2000CA; Packard Instruments, USA). To evaluate the enzymatic activity of PDE2A, the specific inhibitor BAY60–7550 was added to the reaction mix at a final concentration of 0.1 μM.

2.7. Cyclic nucleotide assay

cAMP and cGMP were measured with Direct cAMP/cGMP ELISA kit (Enzo Life Sciences, NY, USA) according to manufacturer's instruction. Brain tissues of WT ($n = 4$) and HET (n = 4) mice were homogenized in 0.1 M HCl with 0.1 % *v/v* Triton X-100 using glass homogenizers. Lysate were then centrifuged at 14,000 *g* for 10 min. Aliquots of 100 μl were analyzed to determine nucleotide levels following the acetylated version of the assay, according to the kit instructions. Aliquots of 5 μl of the supernatant were assayed for protein determination with Bradford assay. Results are referred to a cAMP and cGMP Standard Curves performed together with the cAMP and cGMP Assay. Cyclic nucleotide levels were normalized to the protein content of each sample. Values represent the mean ± SD of at least 3 sample preparations.

2.8. PDE2A and neural nitric oxide synthase (nNOS) immunohistochemistry

Free-floating brain sections were incubated overnight at 4 °C with mouse anti-nNOS monoclonal antibody (1:100; Sigma-Aldrich, Milan, Italy) or with anti-PDE2A rabbit antibody (1:100; Abcam, #ab140650), following the manufacturer instructions. The primary antibody was detected using a biotinylated secondary antibody (Vector Laboratories, Vectastain ABC KIT, Burlingame, CA, USA), and an avidin horseradish peroxidase–diaminobenzidine–H_2O_2 chromogen system (Sigma Fast; Sigma-Aldrich).

Sections were observed and photographed with a light microscope (Olympus BX51), equipped with an automatic micro camera (Leica DC 300 F, Q550 IW Soft). Immunoreaction staining intensity was evaluated in the brain sections, using the Gray Scale Program of the Quantimet Image Processing and Analysis System (Q550 IW Soft). Values were expressed as means ± SD of immunoreactive optical density per unit test area (4.5×10^4 μm^2).

2.9. NADPH-diaphorase histochemistry

A standard histochemical procedure was used for perfusion-fixed brain with paraformaldehyde, as previously reported (Sancesario et al., 2004). Briefly, free-floating brain sections were washed three times with Tris-HCl and incubated for 60–90 min at 37 °C in incubation medium containing 0.1 m Tris-HCl (pH 8.0), 1 mM beta NADPH, 0.2 mM Nitro Blue Tetrazolium and 0.2 % Triton X-100. After histochemical staining, the sections were mounted onto slides, dehydrated, cleared and coverslipped with Permount for light microscope examination. Sections were observed and photographed with a light microscope (Olympus BX51) equipped with an automatic micro-camera (Leica DC 300 F, Q550 IW Soft). 3DSholl and Skeleton analyses were run on the brains of WT ($n = 3$) and HET (n = 3) mice to evaluate the extent of dendritic tree of NADPH positive neurons (5 neurons/area/animal). The following parameters were considered: radial dendritic distance from the soma, total dendritic lengths, and dendritic endpoints of each neuron.

2.10. Statistical analyses

Statistical analyses of behavioral tests were performed with Statistica 12 (StatSoft), by using one-way ANOVAs for independent measures (group) and by two-way ANOVAs for repeated measures in the EPM and ST with Group as between-subjects factor, and Arm/Chamber/Cup as within-subjects' factors. Differences were considered significant at the $p < 0.05$ level.

Statistical analyses of biochemical and morphological data were conducted with GraphPad Prism 9 (Graphpad Software), by using paired or unpaired Student's *t*-test. Normality of data sets was evaluated with Kolmogorov-Smirnov's test. 3D Sholl analysis was evaluated with Mann-Whitney test. Data were represented as mean ± SD and significance level was set at $p < 0.05$ level.

3. Results

3.1. Behavioral findings

HET mice travelled more total distance in the OF arena ($p < 0.01$), exhibited higher mean velocity ($p < 0.01$), and displayed a superior number of rearings ($p < 0.05$) in comparison to WT mice (Fig. 1). No

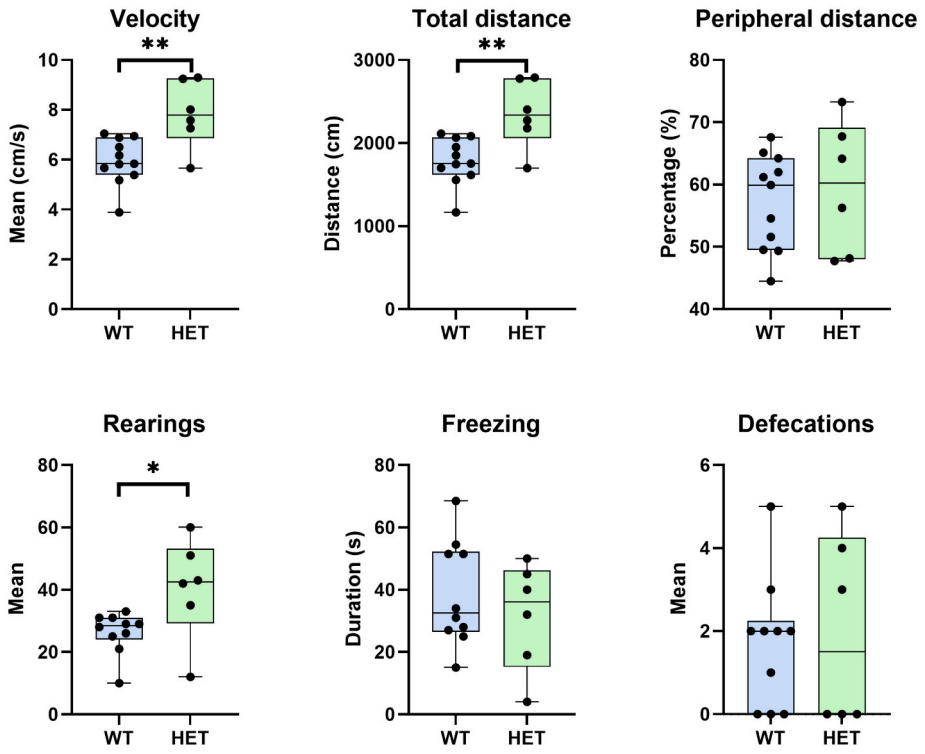

Fig. 1. Open Field. Mean velocity (cm/s). Total distance (cm) travelled by the animal. Percentage of peripheral distance (Distance in the peripheral anulus / Total distance × 100) travelled by the animal. Frequency of Rearings. Times spent in freezing. Defecations during the trial. WT: $n = 11$, HET: $n = 6$. *$P < 0.05$ and **$P < 0.01$.

differences were found in the percentage of distance travelled in the peripheral area of the arena, number of defecations and freezing time shown by the two groups.

Taken together, the increased horizontal and vertical locomotor activities of HET mice, and the absence of modifications in anxiety and emotionality parameters (Bindra and Thompson, 1953) indicate that HET mice exhibited a greater propensity to explore, and the same anxiety levels in comparison to WT.

HET and WT mice buried a similar number of marbles, a clear index that levels of anxiety and compulsive behavior were not affected by the genotype (Supplementary Fig. 1).

HET and WT mice similarly explored open and closed arms of the maze, as indicated by the lack of statistical differences in duration and frequency of arm entries. Both groups spent more time in the closed arms. Both experimental groups displayed a comparable number of defecations. These findings indicate no differences in anxiety levels (Supplementary Fig. 2).

The time spent by HET mice in the Light chamber did not differ from that of WT mice. The same occurred as for the time spent in the Dark chamber, although, as is typically the case, the times in the Dark chamber were longer. No differences between groups were evident in the number of defecations and head dips (Supplementary Fig. 3).

HET and WT mice showed comparable levels of immobility time, a finding indicating no difference in depressive-like behaviors (Supplementary Fig. 4).

No differences were observed in the percentage of spontaneous alternations and frequency of entries displayed by HET and WT mice. These findings indicate that spatial working memory performances were similar in both experimental groups (Supplementary Fig. 5).

HET and WT mice explored more frequently (chamber: $p < 0.05$; cup: $p < 0.001$) and spent more time (chamber: $p < 0.001$; cup: $p < 0.0001$) exploring the chamber and sniffing the cup containing the unfamiliar conspecific, without any difference between groups. These findings demonstrate that the genotype did not affect the preference for social stimulus (Supplementary Fig. 6).

3.2. *Morphological and biochemical findings*

3.2.1. *PDE2A immunohistochemistry*

We studied PDE2A topographical distribution in the brain, to verify whether HET and WT mice displayed regional differences in the PDE2A expression. In WT mice, intense PDE2A brown reaction product immunoreactivity was observed mainly in the cerebral cortex, hippocampus, basal ganglia (in particular, substantia nigra pars reticulata) (Fig. 2), in accordance to Stephenson and colleagues (Stephenson et al., 2009). PDE2A immunoreactivity generally consisted of fine punctate grains densely distributed throughout the neuropil, even if scattered PDE2A positive neuronal bodies were observed in the cerebral cortex and in substantia nigra pars compacta. The pattern of PDE2A immunoreactivity was comparable between the two groups of animals throughout brain areas (Fig. 2A-H), but intensity of immunoreactive product appeared lower in HET mice. Indeed, densitometric analysis demonstrated that the relative intensity of PDE2A immunoreactive product was significantly lower throughout the different brain areas in HET mice, except in the entopeduncular nucleus and nucleus accumbens, compared to corresponding brain areas of WT mice (Fig. 3). These data demonstrate that HET mice have an almost global reduction of PDE2A expression in the brain.

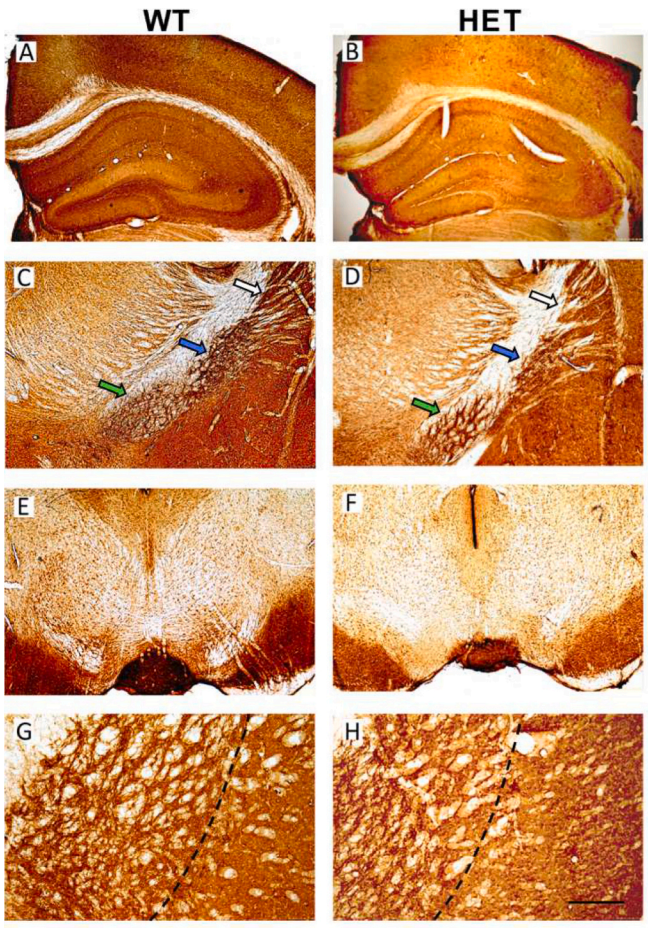

Fig. 2. Low power photomicrographs of PDE2A immunoreactivity in comparative brain sections of WT (A, C, E, G) and HET B, D, F, H) mice in: cerebral cortex and hippocampus (A, B), striatum (arrow white), external globus pallidus (arrow blu), entopeduncular nucleus (arrow green) (C, D), substantia nigra and periaqueductal area (E, F), striatum (on the right in each figure) and external globus pallidus (on the left in each figure) (G, H). Intense PDE2A positive brown reaction product covers gray matter areas, whereas the white matter areas are unstained or just covered by background staining. PDE2A staining appears less intense in HET than in corresponding brain areas of WT. Scale bar in H: A-F = 250 μm; G-H = 100 μm. (For interpretation of the references to colour in this figure legend, the reader is referred to the web version of this article.)

3.2.2. PDE2A protein expression

To evaluate the relative intensity of PDE2A expression in the two groups of animals, Western blot analysis was performed using a specific monoclonal antibody on tissue extracts from whole brain homogenate. A single band of 105 kDa PDE2A immunoreactivity was detected in tissue extracts (Fig. 4A), according to Stephenson and colleagues (Stephenson et al., 2009).

Comparative optical density (O.D.) of Western blotting bands demonstrated that the expression of PDE2A was about 50 % lower in HET mice compared to WT animals (Fig. 4B).

3.2.3. Pde2A mRNA

RT-PCR amplification of *Pde2A* mRNA was performed in the two groups of animals to investigate whether HET mice carried PDE2A changes at the transcriptional level in the brain. The primers gave a strong *Pde2A* amplification in the brain of both groups. However, the relative intensity of *Pde2A* mRNA expression detected in the brain of HET mice was lower than in WT mice (Fig. 4C).

3.2.4. PDE2A hydrolyzing activity

We investigated whether in HET mice the changes in PDE2A expression consistently affected total cGMP-PDE hydrolyzing activity and PDE2A specific activity in tissue extracts. Total cGMP-PDE activity was evaluated as nmol cGMP hydrolyzing activity to inactive 5'GMP/min/mg protein, while specific PDE2A cGMP hydrolyzing activity was evaluated by using PDE2A selective inhibitor BAY 60–7550 at a fixed concentration of 0.1 μM (Schiavi et al., 2022). The amount of total cGMP-PDE activity in the brain was slightly decreased in HET mice, but the decrement was not significant (Fig. 5A). Conversely, the specific activity of PDE2A, obtained from the difference between total cGMP-PDE activity and the residual one in presence of BAY 60–7550, was about 50 % lower in HET mice compared to WT animals (Fig. 5B).

3.2.5. cAMP and cGMP levels

We measured the basal levels of cAMP and cGMP in the two groups of animals to verify whether changes in PDE2A expression and activity in the brain of HET mice actually affected the cyclic nucleotide steady state. Indeed, the cAMP and the CGMP levels appeared increased in whole brain extracts of HET mice compared to WT mice (Fig. 5C, D). However, the mean percentage variations of cGMP and cAMP levels were quite different, much more high for cGMP = 153.23 %, than for cAMP = 16.41 %. These data suggest that the hydrolysis of cAMP and cGMP is differentially regulated in HET mice.

3.2.6. Other PDE proteins

We evaluated whether the differential cAMP/cGMP homeostasis in

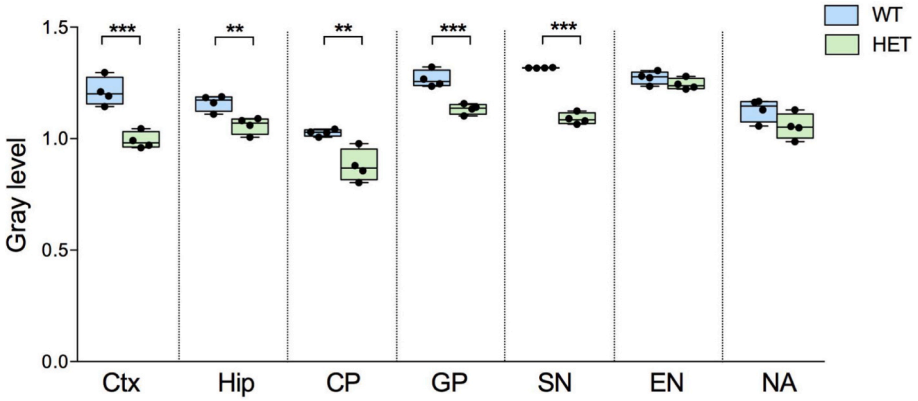

Fig. 3. Densitometric analysis of the PDE2A immunoreactive reaction product in WT and HET mice. The results are expressed as the mean ± SD of the values obtained on each region throughout both hemisphere from five different sections for animal. Optical densities for the cytochemical reaction product were significantly different between almost all corresponding areas of WT and HET mice. Student's *t*-test, $^{**}P < 0.01$, $^{***}P < 0.001$.

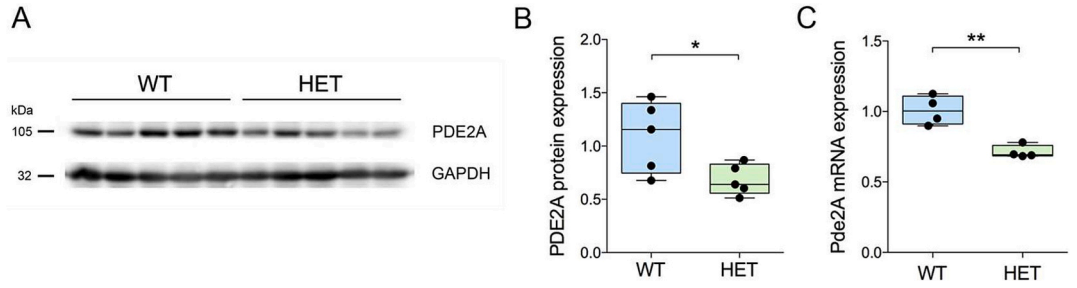

Fig. 4. A) Immunoblots of PDE2A protein content in the brain of WT and HET mice. Thirty micrograms of total protein extract were used. As internal reference standard, the Glyceraldehyde 3-Phosphate Dehydrogenase (GAPDH) was detected in WT and HET mice. B) Densitometric analysis and relative intensity of immunostained bands in the brain of WT and HET mice. PDE2A-specific contents were decreased by about 50 % in HET mice compared with WT mice. The values are the mean ± SD of five different Western blot experiments for the two experimental groups. C) Comparative real-time PCR of *Pde2A* mRNA in the brains of WT and HET mice. Results are expressed as the mean ± SD of the values obtained from four mice in each group. Student's *t*-test, $^{*}P < 0.05$, $^{**}P < 0.01$.

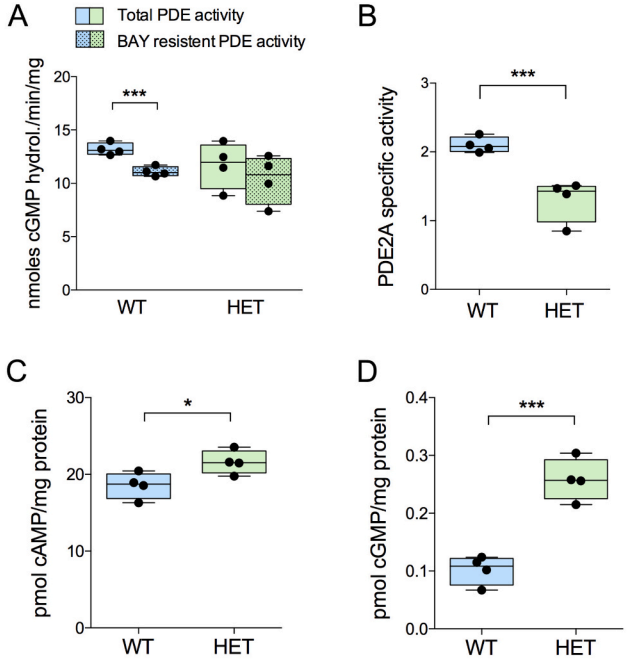

Fig. 5. A) Total PDE activity and BAY60–7550 resistant PDE activity in the brain of WT ($n = 4$) and HET ($n = 4$) mice. Values are expressed as nmol ± SD of cGMP hydrolyzed / min / mg protein, using 1 μM [^{3}H]cGMP as substrate concentration. Measurements were performed on fresh-frozen whole brain hemispheres; each tissue sample was assayed in duplicate. B) PDE2A-specific cGMP degradation measured as the difference of values obtained from brain extracts of WT and HET mice in the absence and presence of BAY60–7550. C—D) cAMP and cGMP contents in the brains of WT ($n = 4$) and HET ($n = 4$) mice. Each tissue sample from each animal was assayed in duplicate. Values are expressed as pmol ± SD of cAMP and cGMP / mg protein. HET mice showed a slight significant increase in the cAMP levels, but a marked increase in the cGMP levels. Student's *t*-test, $^{*}P < 0.05$, $^{***}P < 0.001$.

the brain of HET mice could be dependent on the integrated involvement of other PDEs. Therefore, we performed Western blot analyses of: 1) PDE3A and PDE10A, dual-specificity enzymes that hydrolyze both cAMP and cGMP; 2) PDE5A and PDE9A that selectively hydrolyze cGMP. Western blot analyses were performed by using a monoclonal antibody, specific for each PDE type, on tissue extracts from whole brain homogenate. Single bands of 69 kDa, 70 kDa, 105 kDa, 110 kDa identified respectively PDE9A, PDE10A, PDE5A, PDE3A (Fig.6A).

Comparative optical density (O.D.) of Western blotting bands demonstrated that expression of PDE5A and PDE9A significantly increased, but the expression of PDE3A and PDE10A significantly decreased in HET compared to WT mice (Fig. 6B). These data indicate that the increment of PDE5A and PDE9A was not sufficient to compensate the reduced PDE2A-dependent cGMP catabolism in the brain of HET mice. Therefore, we hypothesized that higher levels of cGMP in the HET brain could be explained by a concurrent increased synthesis. On the other hand, the down regulation of PDE2A is paradoxically associated with an inexplicable reduced expression of PDE3A and PDE10A.

3.2.7. Nitric oxide synthase neurons in HET mice

We evaluated whether the increased levels of cGMP in the brain of HET mice could be dependent, at least in part, on concurrent changes of neuronal nitric oxide synthase (nNOS) expression. nNOS is the predominant physiological source of nitric oxide (NO) in the brain (Garthwaite, 1991), which stimulates the soluble guanylyl cyclase (sGC) to produce the second messenger cGMP. Immunohistochemistry for nNOS labelled a discrete population of medium-sized neurons, fusiform or multipolar in shape, scattered throughout the brain, in particular on the cerebral cortex, striatum (Fig. 7A), and nucleus accumbens. There were no obvious differences in the topographic distribution of nNOS-labelled neurons between HET and WT groups. However, densitometric analysis demonstrated an increase of the nNOS immunostaining in the medium-sized neurons of the striatum and nucleus accumbens, but not of the cortex, in HET compared to WT mice ($p < 0.05$; Fig. 7B, C, D). We then performed Western blot analysis of brain extracts by using a specific nNOS antibody (Fig. 7E), to verify the global nNOS expression in the brain of the two groups of animals. Densitometric analysis demonstrated that nNOS protein contents significantly increased in the brain of HET mice (Fig. 7F), compared to WT animals ($p < 0.05$).

Notably, the distal dendritic arborizations of nNOS neurons appeared shorter in HET mice, compared to nNOS neurons in WT mice (Fig. 7A). To better analyze the morphological characteristics of the nNOS neurons, we used nicotinamide adenine dinucleotide phosphate diaphorase (NADPH-d) histochemical staining technique (Fig. 8A), which allows detecting - with high sensitivity and specificity - fine cytochemical details of nNOS cell bodies, major dendrites and neuritic processes (Figueredo-Cardenas et al., 1996; Sancesario et al., 2000, 1996). However, there is a decreasing gradient of staining intensity between NADPH-d positive cell body and process terminals: therefore signals of the thin process network in the neuropil cannot alway be easily differentiated against the background granular unspecific staining. Actually, we found that nNOS/NADPH-d positive neurons of HET mice ($n = 3$) exhibited reduced cumulative dendritic length, and fewer dendritic endpoints in the cerebral cortex, striatum and nucleus accumbens compared to WT mice ($n = 3$) (Fig. 8B).

4. Discussion

We found that the haploinsufficiency of PDE2A activates complex

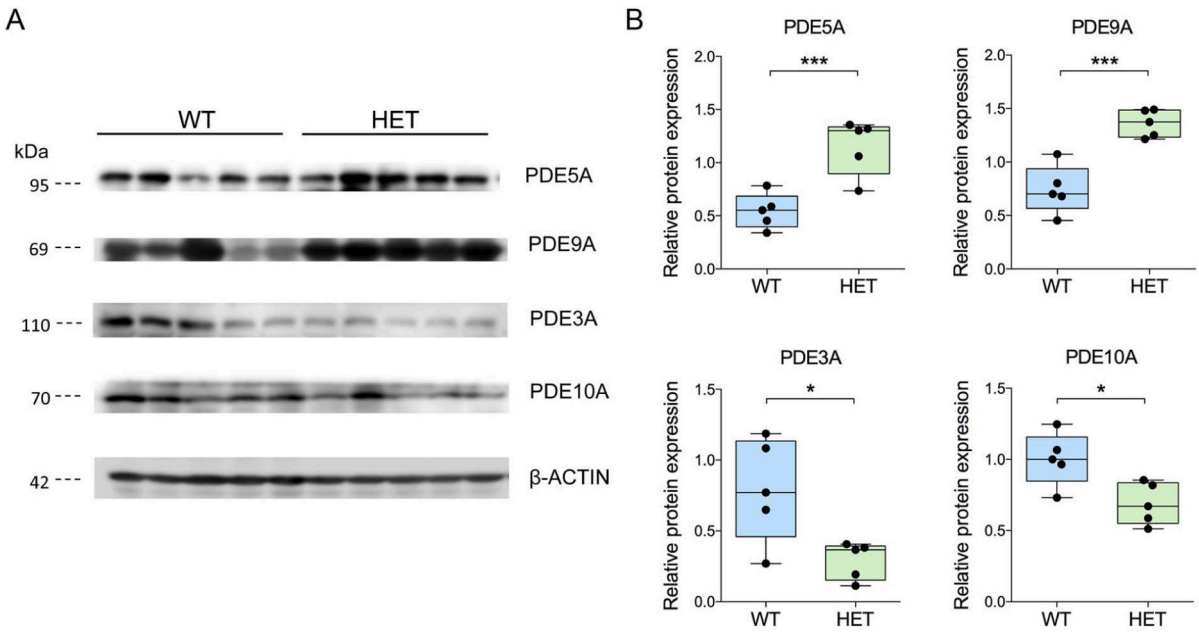

Fig. 6. A) Immunoblots of PDE3A, PDE5A, PDE9A, PDE10A. Thirty micrograms of total protein extract were used from the brain of WT ($n = 5$) and HET ($n = 5$) mice. As internal reference standard, the β-actin content was detected. B) Densitometric analysis and relative intensity of immunostained bands. In the brain of HET mice PDE5A and PDE9A specific contents were increased, but the PDE3A and PDE10A were significantly decreased. The values are the mean ± SD of five different Western Blot experiments per experimental group. Student's *t*-test, $^{*}P < 0.05$, $^{***}P < 0.001$.

interactions with other PDEs, but it is also specifically coupled with increased expression nNOS, to compensate changes of PDE2A dependent cAMP and cGMP metabolism.

4.1. Biochemical and immunohistochemical findings

Biochemical and immunohistochemical findings of the present research demonstrate that HET mice display 50 % reduction in PDE2A protein expression and activity in comparison with WT mice. Therefore, we were expecting that the reduced expression of PDE2A in HET mice would have determined comparable increased levels of the second messengers cAMP and cGMP, given that PDE2A catabolizes both cyclic nucleotides. Unexpectedly, the mean percentage increases of the two cyclic nucleotides levels were highly differentiated in HET mice: the cAMP elevated just to 16.41 %, whereas the cGMP wheeled to 153.23 %.

4.1.1. Cross-talk between the cAMP and cGMP signaling

It is well-known that in physiological conditions in rodent brain the baseline levels of cAMP are much higher (about 20 pmol/mg proteins) than the cGMP levels (about 0.1 pmol/mg protein) (Giorgi et al., 2008). To understand the compensatory mechanisms preferentially maintaining cAMP homeostasis in HET mice, we should first consider the differential affinity of PDE2A for the cAMP (K_m, ~30 μM) and for cGMP (K_m, ~10 μM): actually the lower is the value of K_m for cGMP, the higher is its affinity for PDE2A compared to cAMP, and vice versa. Moreover, we should consider the allosteric characteristics of the enzyme PDE2A that can bind both cAMP and cGMP simultaneously, but selectively at two distinct sites, named respectively active and effector: upon binding the cGMP at the effector site, PDE2A changes its conformational structure, and it increases the affinity of the active site to bind the cAMP, so improving cAMP metabolism. Therefore, at physiological concentrations, cGMP is the preferred substrate for PDE2A effector site, which can stimulate PDE2A-mediated cAMP hydrolysis. Actually, nanomolar to micromolar concentrations of cGMP can accelerate cAMP hydrolysis 7–14 folds, with K_a for cGMP of 0.36 μM. However, at higher concentrations (~10 μM) cGMP can compete with cAMP binding at the catalytic site and can thus inhibit cAMP hydrolysis (Martins et al., 1982; Weston et al., 2003). According to the functional characteristics of PDE2A, in HET mice the higher cGMP levels (HET 0.26 ± 0.036 SD > WT 0.10 ± 0.025 SD pmol/mg protein) can represent the preferred substrate for PDE2A effector site, stimulating the cAMP-hydrolyzing activity of the active site. In such a way, the reduced content of PDE2A in HET mice could be compensated by the increased cGMP-stimulated cAMP hydrolyzing activity, which in turn could contribute, at least partially, to maintain a limited increase of cAMP content (WT 18.55 ± 1.71 SD > HET 21.59 ± 1.54 SD pmol/mg protein).

4.1.2. Interactions of PDE2A with other PDEs

We were expecting that the reduced expression of PDE2A in the brain of HET mice could be compensated by an increased expression of other dual-specificity enzymes, such PDE3 and PDE10A. Conversely, in association with the reduced expression of PDE2A, we found a reduced content of PDE3A and PDE10A in the brain of HET mice. Although these results are not easily interpretable as compensatory mechanisms, let's consider the specific functional characteristics of each PDE. Unlike PDE2A that is stimulated by cGMP to hydrolyze cAMP, cAMP hydrolyzing activity of PDE3A is inhibited by cGMP (Shakur et al., 2001). Therefore, the PDE3A downregulation in HET mice may be considered a balance mechanism in the presence of high levels of cGMP, oppositely correlated to the cGMP-stimulated cAMP hydrolyzing activity of PDE2A.

On the other hand, PDE10A has high affinity for cAMP, so that, in spite of its dual-specificity, it primarily acts as a cAMP-specific PDE, and only in the case of very low cAMP concentrations it can contribute to cGMP degradation (Jäger et al., 2012). Therefore, to interpret the reduced PDE10A expression correlated with the PDE2A deficiency in HET mice, we may advance that the cGMP-stimulated cAMP hydrolyzing activity of PDE2A has a predominant role to maintain cAMP homeostasis in HET mice, with secondary compensatory downregulation of PDE3A and PDE10A. Accordingly, the high levels of cGMP in HET mice could be explained, at least in part, by the reduced PDE3A and PDE10A expression, associated with PDE2A deficiency.

Thereafter, we explored the expression of PDE5A and PDE9A that selectively hydrolyze cGMP. PDE5A exerts a major role in degrading cGMP produced by nitric oxide (NO) as well as by the natriuretic

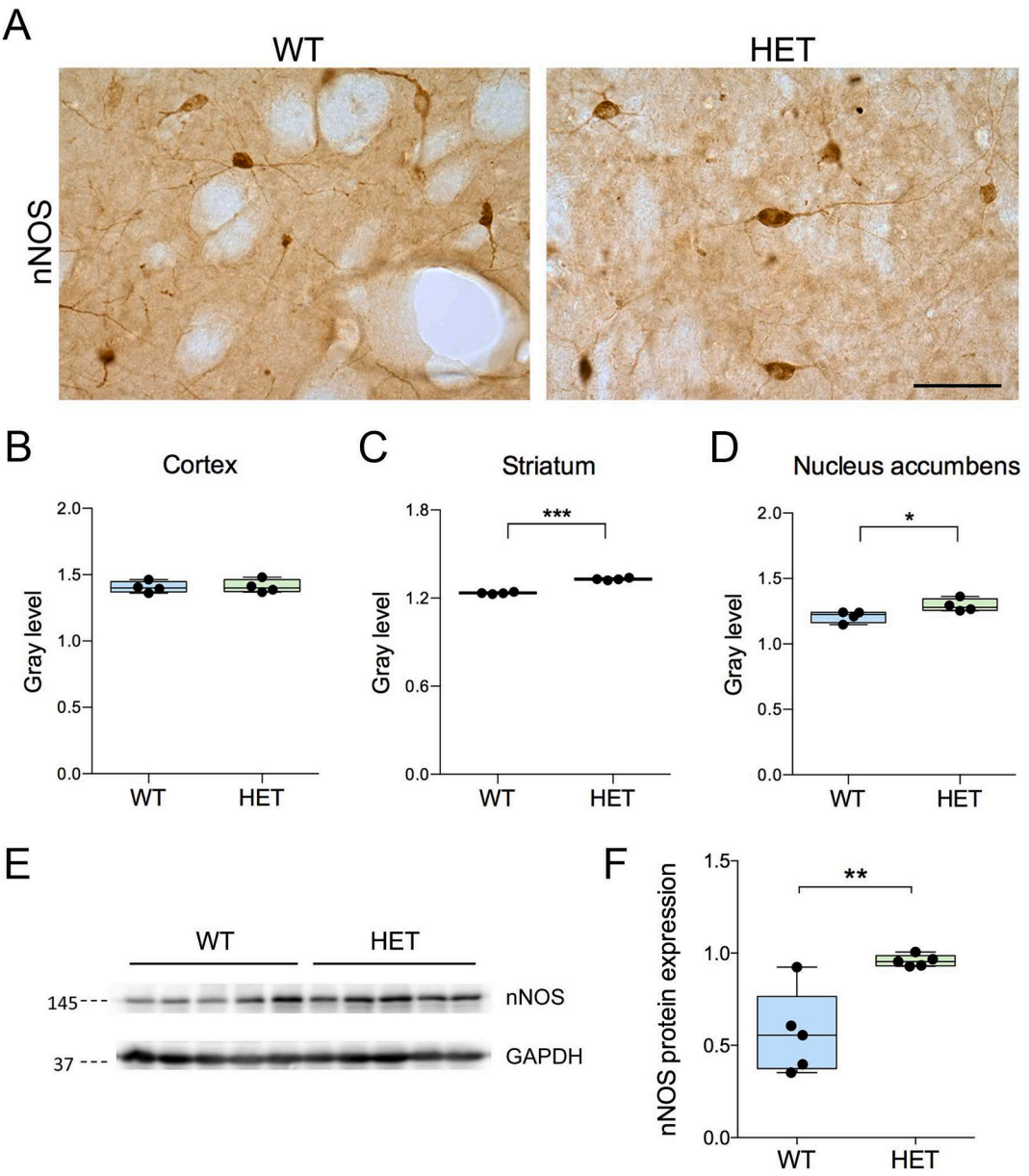

Fig. 7. A) Photomicrographs of nNOS-immunoreactive neurons in vibratome sections (40 μm thick) from the striatum of WT and HET mice. The number of nNOS neuronal bodies appears similar in both groups of mice, however their nNOS immunoreactivity appears increased in HET mice. Scale bar, 100 μm. B, C, D) Densitometric analyses of the nNOS immunoreactivity in neuronal bodies on different brain regions of WT ($n = 4$) and HET ($n = 4$) mice. The results are expressed as mean ± SD of the values obtained on each region throughout both hemisphere from five different sections. Optical density for the cytochemical reaction product was significantly increased in nNOS neurons in the striatum and in the nucleus accumbens but not in the cerebral cortex of HET mice. E) Immunoblots of nNOS. Thirty micrograms of total protein extract were used from the brains of WT ($n = 5$) and HET ($n = 5$) mice. As internal reference standard, the GAPDH was detected. F) nNOS densitometric analysis and relative intensity of immunostained bands. In the brain of HET mice nNOS specific contents were increased. The values are the mean ± SD of five different Western Blot experiments per experimental group. Student's *t*-test, $^{*}P < 0.05$, $^{**}P < 0.01$, $^{***}P < 0.001$.

peptides, while PDE9A only regulates NO-induced cGMP increase (Bobruskin et al., 1991). However, the consistent up-regulation of PDE5A and PDE9A, actually occurring in HET mice, did not result sufficient to compensate for the reduced cGMP hydrolysis by PDE2A, and likely also by PDE3A and PDE10A. Moreover, we have to consider that, despite the variations in the protein levels of these PDEs, total cGMP-hydrolizing activity is very similar between WT and HET (Fig. 5A). This might suggest that the increased intracellular cGMP concentration is due to a problem in its biosynthesis rather than in its degradation. Therefore, we argue that the increased cGMP levels of HET mice may be partly related to an up-regulation of NO, which is the main source of cGMP synthesis in the brain.

4.1.3. PDE2A, nNOS and NO-induced cGMP synthesis

NO is a multifaced signaling molecule, with very short half-life of 1–10 s, produced by three distinct isoforms of the enzyme nitric oxide synthase (NOS): endothelial (eNOS), inducible (iNOS), and neuronal (nNOS). In the brain, nNOS selectively characterizes a subset of interneurons widely distributed in the cerebral cortex, thalamus, hippocampus, and basal ganglia (Chong et al., 2019). In HET mice, we found an increased content of nNOS, particularly significant in the striatal neurons. Notably, the striatal neurons exhibited a significant increase of nNOS content in neural bodies but a decrease of their dendritic arbor. By examining the morpho-chemical changes in nNOS neurons, specifically in the striatum, we aimed to gain insight into how they may be connected to the high levels of cGMP and to PDE2A changes in HET mice.

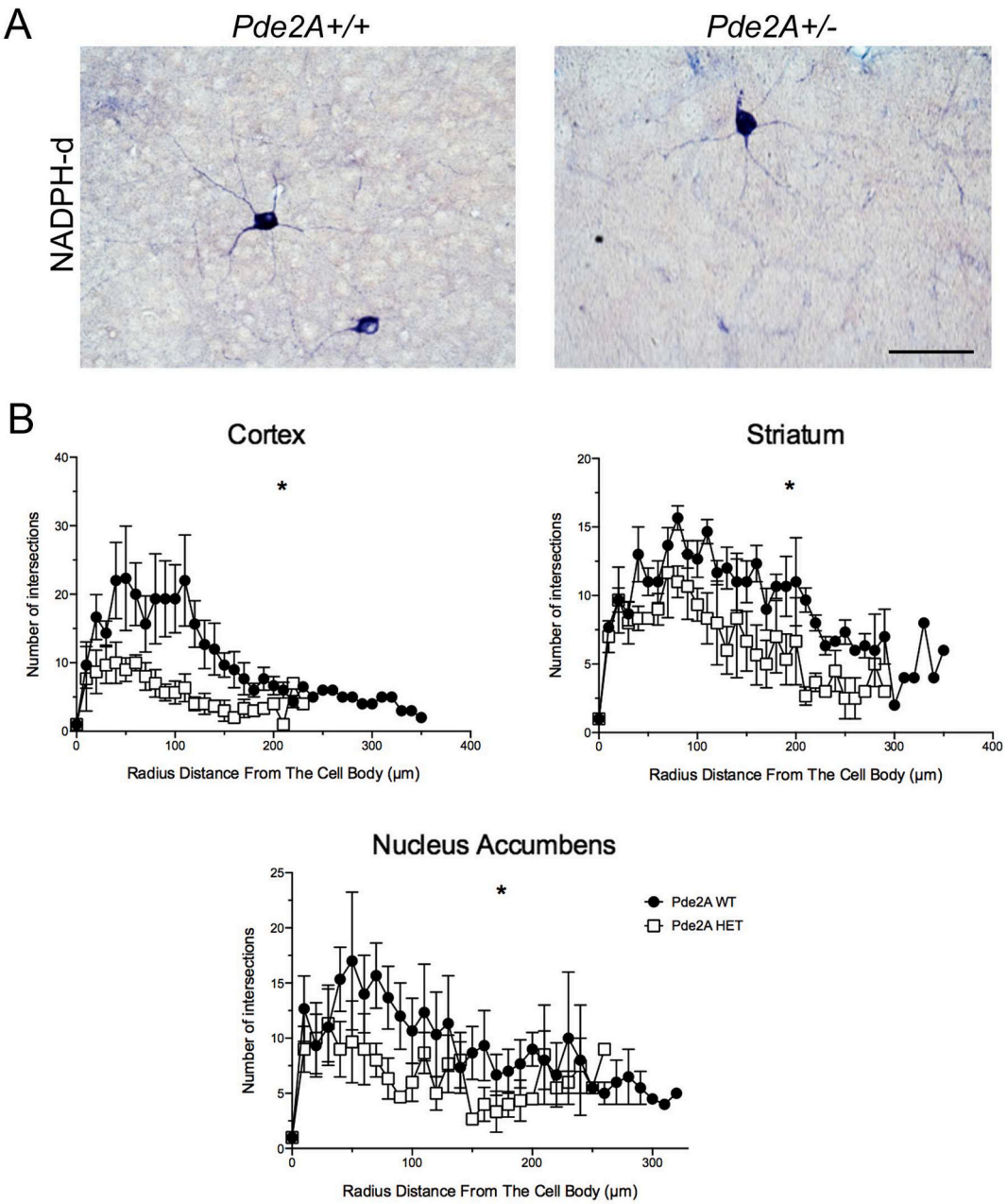

Fig. 8. A) Photomicrographs of NDPH-d positive neurons in 40 µm-thick vibratome sections from the striatum of WT and HET mice. The number of NADPH-d neuronal bodies appears similar in both groups of mice, however the extent of their dendritic arborizations appears reduced in HET mice. Scale bar, 100 µm. B) Plot of the mean number of intersections along the radial distance from the neuronal soma of NADPH-d neurons on different brain regions, indicating reduced dendritic branching of neurons (5 neurons/region/animal) in HET mice ($n = 3$) compared with neurons in corresponding areas (5 neurons/region/animal) in WT ($n = 3$). Mann-Whitney test, $^*P < 0.05$.

nNOS interneurons make synaptic contacts on the dendritic spines of the striatal medium-sized spiny neurons (MSNs) (Morello et al., 1997). NO produced by nNOS interneurons diffuses throughout the striatal complex, and activates NO soluble guanylyl cyclase (sGC) to produce cGMP into the dendrites of MSNs, modulating cortico-striatal synaptic plasticity (Sammut et al., 2010; Wang and Robinson, 1997). Indeed, the NO/cGMP pathway plays a critical role in inducing cortico-striatal long-term depression (LTD) in MSNs (Calabresi et al., 1999). Moreover, NO via a sGC-cGMP dependent mechanism reduces the cAMP signals in both striato-nigral and striato-pallidal MSNs through the activation of PDE2A (Polito et al., 2013). Therefore, the increased nNOS content in striatal interneurons may express also an increased synthesis of NO, leading to NO-induced cGMP high levels in MSNs, and up-regulating PDE2A-related hydrolysis of cAMP in HET mice. Therefore, our data advance a compensatory functional link between the PDE2A down-regulation and nNOS-cGMP up-regulation in HET mice.

4.1.4. PDE2A/nNOS inverse relationship

It is worth to note that: a) the levels of PDE2A are decreased while those of nNOS are increased in HET mice with haploinsufficiency; b) oppositely, levels and activity of PDE2A are increased in genetic and environmental preclinical models of autism (Maurin et al., 2019; Schiavi et al., 2022), while the nNOS expression is severely diminished in postnatal neocortex of human patients affected by fragile X syndrome, as well as in two mouse models of autism (East et al., 1996; Wang et al., 2018). These data raise the question whether PDE2A is a negative

regulator of nNOS, or whether PDE2A and nNOS could be mutual regulator each other. Gaining insight into the regulatory mechanism involved between the opposite PDE2A-nNOS changes would provide novel strategies for manipulating nNOS and PDE2A to therapeutic modalities in the future.

4.1.5. PDE2A and nNOS neuron dendrites

Although the NADPH-d positive distal thin process network cannot be reliably evaluated in the neuropil, because herein the signal to noise ratio is high in our work, nNOS qualitative and NADPH-d quantitative morphometric evaluations demonstrate that the nNOS-NADPH-d positive neurons display apparent shorter dendritic arborization in the cerebral cortex, the striatum and nucleus accumbens. In particular, it is not easy to reconcile the increased content of nNOS enzyme in neuronal bodies with the reduced dendritic arborization of nNOS neurons in the striatum of HET mice, as we found in the present research. We have to consider that striatal nNOS interneurons are innervated by glutamatergic projections from the cortex, and contain ionotropic glutamate receptors, expressing in particular a distinct NMDA receptor phenotype (East et al., 1996). Several biochemical and pharmacological studies demonstrated that glutamate, acting via NMDA receptors, is one of the most potent activators of nNOS (Garthwaite, 1991; Weiss et al., 1998). In turn, NMDA receptors are under the control of cAMP/protein kinase A (PKA), which induces direct phosphorylation of NMDA receptors and potentiates their activity (Skeberdis et al., 2006). This PKA/NMDA positive feed-back is under the control of the NO/cGMP signaling, which activating PDE2A reduces the cAMP signals and, downstream, the PKA activation. However, the NO/cGMP signaling is restricted to activate PDE2A hydrolyzing cAMP transients, synthetized by adenylyl cyclase stimulation, but has no effect on basal cAMP signal (Polito et al., 2013).

The specific role of PDE2A in regulating the cAMP transients can represent the key point to interpret the different changes of cAMP and cGMP, as well as the reduced arborization of nNOS neurons we detected in HET mice. We found a slightly significant increment of total cAMP levels in the brain of HET mice in comparison to WT mice, but this result likely represents just basal cAMP levels that are not representative of the transient rises of cAMP in HET mice. Therefore, the up-regulation of the NO/cGMP signaling could not be sufficient to completely compensate for the PDE2A deficit in HET mice, and probably results in partially uncontrolled transient rises of the cAMP levels and unusual hyperactivation of PKA/NMDA positive feed-back.

Hyperactive NMDA receptors increase intracellular Ca^{2+} concentration, up-regulate nNOS, and initiate a cascade of signaling pathways leading to glutamate excitotoxicity (Kritis et al., 2015). It is well known that cortical neurons exposed to excess of extracellular glutamate (100 μM) display reduced dendrite growth, which occurs in the absence of cell death (Monnerie et al., 2003). Moreover, the excitotoxic injury produced by NMDA receptor activation can be amplified by NO released by nNOS neurons (Schulz et al., 1995). Therefore, the reduced dendritic arborization of nNOS neurons of HET mice could depend on an excessive PKA/NMDA activation and subsequent excitotoxicity. This hypothesis is supported by the recent paper by Delhaye and colleagues (Delhaye et al., 2024), demonstrating an increased phosphorylation level of hippocampal GluR1of HET mice, in association with reduced mGluR-dependent LTD (Delhaye et al., 2024). Notably, such LTD reduction could be sustained also by the increased content of PDE5 and PDE9 we found in HET mice, considering that the PDE5 inhibitor Zaprinast can activate LTD (Calabresi et al., 1999). Therefore, in HET mice a deficit of LTD may predispose to a long-lasting increase of synaptic strength, long-term potentiation (LTP) and to glutamate neurotoxicity. Future studies should clarify whether in HET mice there is an imbalance between LTD and LTP, and whether reduced dendritic arborization also affects other neuronal types than nNOS neurons

4.2. PDE2A deficiency and behavioral phenotype

To characterize the behavioral phenotype of HET mice, various behavioral domains have been assessed through a battery of tests covering a wide range of behaviors, such as explorative activity, motor abilities, anxiety levels, depression-like behavior, spatial working memory, and social behavior. HET mice displayed increased horizontal and vertical locomotor activity and increased velocity in foraging the OF arena, presumably related to their greater propensity to explore novel environments. The superior explorativity of HET mice was not related to superior levels of anxiety, given OF (as for percentage of peripheral distance), MBT, L/D, and EPM tests indicated no differences in anxiety levels between groups. Even spatial working memory (in Y-maze), preference for social stimulus (in ST) as well as depressive-like (in TST) and compulsive (in MBT) behaviors were similar in both experimental groups. Therefore, HET mice manifested a behavioral phenotype characterized by enhanced explorativity, without evident deficits in mnesic and sociability behaviors, as well as in anxiety levels and depressive-like behaviors.

Integrating the behavioral performances displayed by the HET mice of the present study with those of the HET mice described by Delhaye and colleagues (Delhaye et al., 2024), it appears that the HET mice's behavioral phenotype is characterized by: 1) developmental maturation retard and early communicative deficits at PND10, reduced social interactions at PND 30, and memory impairment at PND 60 (Delhaye et al., 2024); 2) enhanced tendencies to explore new environments, without evident cognitive and sociability deficits at PND 90–120 (the current study). Furthermore, HET mice do not display difference in anxiety levels compared to WT mice at PND 60 as well as at PND 90–120.

Although overall the behavioral findings of the present research are aligned with those of the prior study, some divergent findings are noted. Namely, HET mice exhibited deficits in working and short-term memory (novel object recognition task) at PND 60 (Delhaye et al., 2024), but their spatial working memory (Y-maze) was not damaged at PND 90–120; their vertical locomotor activity was increased at PND 90–120 but not at PND 60; and finally, they displayed reduced social interactions at PND 60, but exhibited a significant preference for social stimulus at PND 90–120. These findings may be interpreted by proposing that HET mice's memory deficits do not reflect a general mnesic impairment, that PDE2A activity is critical for specific social behaviors, as social interactions, but not for others, as the salience of social stimulus, and that some age-related changes may occur in specific behavioral domains.

A key factor to explain these differences could be the age of testing. In fact, while in the paper of Delhaye et al. (2024) the HET mice were tested at $\leq$ PND 60, in the present research HET mice were tested at $>$ PND 90–120. Thus, the behavioral phenotype might be changed with age when compensatory mechanisms might be able to rescue some deficits, or conversely detrimental mechanisms might be able to disclose others. Furthermore, as distinct HET mice groups were used in these two studies, this might have contributed to some of the divergent findings. Long-term studies, tracking the development of single HET individuals over their whole lifetime, will allow overcoming these troubles.

4.2.1. PDE2A deficiency and neuro-anatomical correlates of behavioral phenotype

Although a global reduction of PDE2A occurs in the HET mice brain, a marked increase of nNOS expression has been found only in striatal nNOS interneurons of HET mice, but not in cerebral cortex. On the other hand, the behavioral phenotype of adult HET mice is specifically characterized by increased locomotor activity, related to greater propensity to explore novel environments; no other neurological signs were detected in the adult HET mice. Therefore, HET mice at a time show increased nNOS expression in the striatum, and increased exploratory behavior.

We now will try to correlate the biochemical and morphological changes detected in the brain of HET mice with their behavioral phenotype. The neural substrates for exploratory behavior have been in general identified in the basal ganglia (Chakravarthy, 2013). Moreover, compelling evidence demonstrates that the NO-sGC-cGMP signaling pathway in the striatum plays a key role in the regulation of motor functions (Del Bel et al., 2005; Lorenc-Koci and Czarnecka, 2013). Indeed, a reduction of striatal nNOS/cGMP pathway associated with reduced motor activity occurs in 6-OHDA rat model of Parkinson's disease (Sancesario et al., 2004). PDE2A inhibitors are tested for the treatment of Parkinson's disease (Wang et al., 2022). Finally, neurochemical correlates of the effects of PDE2A inhibitors are represented by increased NO-cGMP pathway, which is thought to be activated by NMDA receptors (Masood et al., 2009). Therefore, we suggest that the increased locomotor and exploratory activity of adult HET mice can be dependent on the upregulation of the nNOS/NO/cGMP signaling in the striatum.

5. Conclusions

Adult HET mice at the age of 3–4 months show high exploratory phenotype and normal social interactions and cognitive capacity, suggesting they have acquired compensatory mechanisms of PDE2A deficiency. In fact, although PDE2A expression and activity were significantly reduced by 50 %, in adult HET mice, the cAMP levels were slightly increased in the brain, whereas only the cGMP levels were markedly increased. Paradoxically, the deficiency of PDE2A was coupled with the deficiency also of the other dual-specificity enzymes, PDE3A and PDE10A, and the high cGMP levels coexisted with the increased expressions of cGMP-specific PDE5A and PDE9A. These apparently contradictory data suggest that a complex network of different factors is involved in HET brain to acquire a new homeostatic equilibrium for cAMP and cGMP. Interestingly, the main finding of the present study is the discovery of the inverse regulation of PDE2A and nNOS (low levels of PDE2A vs. high levels of nNOS) occurring in the HET mice, whereas high levels of PDE2A and low levels of nNOS were found in models of autism, suggesting PDE2A as a negative regulator of nNOS. Such PDE2A/nNOS relation could represent an auto-regulatory mechanism of PDE2A function, since cGMP can stimulate PDEA2-mediated cAMP hydrolysis. However, NO released by nNOS neurons can also amplify NMDA receptor activation, impairing the scaling process of LTD (Delhaye et al., 2024), and leading finally to glutamate excitotoxic injury (Kritis et al., 2015), and to reduced dendritic arborization of nNOS neurons in the striatum (present paper), which can occur in the absence of cell death (Monnerie et al., 2003).

Our study unraveling the complex interrelations among changes of PDE2A, other PDEs, and nNOS increased NO synthesis, represents another brick of knowledge on PDE2A functions and its possible role as therapeutic target in ASD and other pathophysiological conditions.

Funding

This work was supported by Sapienza University # AR122181686381EC and #RM120172A3B45898.

CRediT authorship contribution statement

Ana Gabriela de Oliveira do Rêgo: Visualization, Methodology, Investigation, Formal analysis, Data curation. **Francesca D'Amico:** Methodology, Investigation, Formal analysis. **Vincenza D'Angelo:** Methodology, Investigation. **Silvia Cardarelli:** Writing – review & editing, Investigation, Data curation. **Debora Cutuli:** Investigation, Formal analysis. **Davide Decandia:** Investigation, Data curation. **Eugenia Landolfo:** Writing – review & editing, Formal analysis. **Laura Petrosini:** Writing – review & editing, Formal analysis, Data curation. **Manuela Pellegrini:** Supervision, Resources, Funding acquisition. **Marcello D'Amelio:** Writing – review & editing. **Nicola Biagio Mercuri:** Writing – review & editing. **Mauro Giorgi:** Writing – review & editing, Supervision, Funding acquisition, Data curation, Conceptualization. **Giuseppe Sancesario:** Writing – original draft, Validation, Supervision, Conceptualization.

Declaration of competing interest

All the authors do not report any disclosures.

Data availability

No data was used for the research described in the article.

Appendix A. Supplementary data

Supplementary data to this article can be found online at https://doi.org/10.1016/j.nbd.2024.106781.

References

Assenza, M.R., Barbagallo, F., Barrios, F., Cornacchione, M., Campolo, F., Vivarelli, E., Gianfrilli, D., Auletta, L., Soricelli, A., Isidori, A.M., Lenzi, A., Pellegrini, M., Naro, F., 2018. Critical role of phosphodiesterase 2A in mouse congenital heart defects. Cardiovasc. Res. 114, 830–845. https://doi.org/10.1093/cvr/cvy030.

Barbagallo, F., Rotilio, V., Assenza, M.R., Aguanno, S., Orsini, T., Putti, S., Isidori, A.M., Lenzi, A., Naro, F., De Angelis, L., Pellegrini, M., 2020. PDE2A is indispensable for mouse liver development and hematopoiesis. Int. J. Mol. Sci. 21, 2902. https://doi.org/10.3390/ijms21082902.

Bindra, D., Thompson, W.R., 1953. An evaluation of defecation and urination as measures of fearfulness. J. Comp. Physiol. Psychol. 46, 43–45. https://doi.org/10.1037/h0057952.

Bobruskin, I.D., Medvedeva, M.V., Severin, E.S., 1991. cGMP-activated phosphodiesterase from human brain: kinetic and regulatory properties. Biokhimiia 56, 999–1010.

Boyken, J., Grønborg, M., Riedel, D., Urlaub, H., Jahn, R., Chua, J.J.E., 2013. Molecular profiling of synaptic vesicle docking sites reveals novel proteins but few differences between glutamatergic and GABAergic synapses. Neuron 78, 285–297. https://doi.org/10.1016/j.neuron.2013.02.027.

Calabresi, P., Gubellini, P., Centonze, D., Sancesario, G., Morello, M., Giorgi, M., Pisani, A., Bernardi, G., 1999. A critical role of the nitric oxide/cGMP pathway in corticostriatal long-term depression. J. Neurosci. 19, 2489–2499. https://doi.org/10.1523/JNEUROSCI.19-07-02489.1999.

Cardarelli, S., Biglietto, M., Orsini, T., Fustaino, V., Monaco, L., de Oliveira do Rêgo, A. G., Liccardo, F., Masciarelli, S., Fazi, F., Naro, F., De Angelis, L., Pellegrini, M., 2024. Modulation of cAMP/cGMP signaling as prevention of congenital heart defects in Pde2A deficient embryos: a matter of oxidative stress. Cell Death Dis. 15, 169. https://doi.org/10.1038/s41419-024-06549-1.

Chakravarthy, V.S., 2013. A model of the neural substrates for exploratory dynamics in basal ganglia. Prog. Brain Res. 202, 389–414. https://doi.org/10.1016/B978-0-444-62604-2.00020-4.

Chong, P.S., Poon, C.H., Fung, M.L., Guan, L., Steinbusch, H.W.M., Chan, Y.-S., Lim, W. L., Lim, L.W., 2019. Distribution of neuronal nitric oxide synthase immunoreactivity in adult male Sprague-Dawley rat brain. Acta Histochem. 121, 151437. https://doi.org/10.1016/j.acthis.2019.08.004.

D'Angelo, V., Castelli, V., Giorgi, M., Cardarelli, S., Saverioni, I., Palumbo, F., Bonsi, P., Pisani, A., Giampà, C., Sorge, R., Biagioni, S., Fusco, F.R., Sancesario, G., 2017. Phosphodiesterase-10A inverse changes in Striatopallidal and Striatoentopeduncular pathways of a transgenic mouse model of DYT1 dystonia. J. Neurosci. 37, 2112–2124. https://doi.org/10.1523/JNEUROSCI.3207-15.2016.

Del Bel, E.A., Guimarães, F.S., Bermúdez-Echeverry, M., Gomes, M.Z., Schiaveto-de-souza, A., Padovan-Neto, F.E., Tumas, V., Barion-Cavalcanti, A.P., Lazzarini, M., Nucci-da-Silva, L.P., de Paula-Souza, D., 2005. Role of nitric oxide on motor behavior. Cell. Mol. Neurobiol. 25, 371–392. https://doi.org/10.1007/s10571-005-3065-8.

Delhaye, S., Jarjat, M., Boulksibat, A., Sanchez, C., Tempio, A., Turtoi, A., Giorgi, M., Lacas-Gervais, S., Baj, G., Rovere, C., Trezza, V., Pellegrini, M., Maurin, T., Lalli, E., Bardoni, B., 2024. Defects in AMPAR trafficking and microglia activation underlie socio-cognitive deficits associated to decreased expression of phosphodiesterase 2 a. Neurobiol. Dis. 191, 106393. https://doi.org/10.1016/j.nbd.2023.106393.

Doummar, D., Dentel, C., Lyautey, R., Metreau, J., Keren, B., Drouot, N., et al., 2020. Biallelic PDE2A variants: a new cause of syndromic paroxysmal dyskinesia. Eur. J. Hum. Genet. 28, 1403–1413. https://doi.org/10.1038/s41431-020-0641-9.

East, S.J., Parry-Jones, A., Brotchie, J.M., 1996. Ionotropic glutamate receptors and nitric oxide synthesis in the rat striatum. Neuroreport 8, 71–75. https://doi.org/10.1097/00001756-199612200-00015.

Farmer, R., Burbano, S.D., Patel, N.S., Sarmiento, A., Smith, A.J., Kelly, M.P., 2020. Phosphodiesterases PDE2A and PDE10A both change mRNA expression in the human brain with age, but only PDE2A changes in a region-specific manner with psychiatric disease. Cell. Signal. 70. https://doi.org/10.1016/j.cellsig.2020.109592.

Figueredo-Cardenas, G., Morello, M., Sancesario, G., Bernardi, G., Reiner, A., 1996. Colocalization of somatostatin, neuropeptide Y, neuronal nitric oxide synthase and NADPH-diaphorase in striatal interneurons in rats. Brain Res. 735, 317–324. https://doi.org/10.1016/0006-8993(96)00801-3.

Francis, S.H., Blount, M.A., Corbin, J.D., 2011. Mammalian cyclic nucleotide phosphodiesterases: molecular mechanisms and physiological functions. Physiol. Rev. 91 (2), 651–690. https://doi.org/10.1152/physrev.00030.2010.

Garthwaite, J., 1991. Glutamate, nitric oxide and cell-cell signalling in the nervous system. Trends Neurosci. 14, 60–67. https://doi.org/10.1016/0166-2236(91)90022-m.

Giorgi, M., D'Angelo, V., Esposito, Z., Nuccetelli, V., Sorge, R., Martorana, A., Stefani, A., Bernardi, G., Sancesario, G., 2008. Lowered cAMP and cGMP signalling in the brain during levodopa-induced dyskinesias in hemiparkinsonian rats: new aspects in the pathogenetic mechanisms. Eur. J. Neurosci. 28, 941–950. https://doi.org/10.1111/j.1460-9568.2008.06387.x.

Haidar, Z., Jalkh, N., Corbani, S., Abou-Ghoch, J., Fawaz, A., Mehawej, C., Chouery, E., 2020. A homozygous splicing mutation in PDE2A in a family with atypical Rett syndrome. Mov. Disord. 35, 896–899. https://doi.org/10.1002/mds.28023.

Jäger, R., Russwurm, C., Schwede, F., Genieser, H.-G., Koesling, D., Russwurm, M., 2012. Activation of PDE10 and PDE11 Phosphodiesterases*. J. Biol. Chem. 287, 1210–1219. https://doi.org/10.1074/jbc.M111.263806.

Kritis, A.A., Stamoula, E.G., Paniskaki, K.A., Vavilis, T.D., 2015. Researching glutamate – induced cytotoxicity in different cell lines: a comparative/collective analysis/study. Front. Cell. Neurosci. 9. https://doi.org/10.3389/fncel.2015.00091.

Lorenc-Koci, E., Czarnecka, A., 2013. Role of nitric oxide in the regulation of motor function. An overview of behavioral, biochemical and histological studies in animal models. Pharmacol. Rep. 65, 1043–1055. https://doi.org/10.1016/s1734-1140(13)71464-6.

Martins, T.J., Mumby, M.C., Beavo, J.A., 1982. Purification and characterization of a cyclic GMP-stimulated cyclic nucleotide phosphodiesterase from bovine tissues. J. Biol. Chem. 257, 1973–1979.

Masood, A., Huang, Y., Hajjhussein, H., Xiao, L., Li, H., Wang, W., Hamza, A., Zhan, C.G., O'Donnell, J.M., 2009. Anxiolytic effects of phosphodiesterase-2 inhibitors associated with increased cGMP signaling. J. Pharmacol. Exp. Ther. 331 (2), 690–699. https://doi.org/10.1124/jpet.109.156729.

Maurin, T., Melancia, F., Jarjat, M., Castro, L., Costa, L., Delhaye, S., Khayachi, A., Castagnola, S., Mota, E., Di Giorgio, A., Servadio, M., Drozd, M., Poupon, G., Schiavi, S., Sardone, L., Azoulay, S., Ciranna, L., Martin, S., Vincent, P., Trezza, V., Bardoni, B., 2019. Involvement of phosphodiesterase 2A activity in the pathophysiology of fragile X syndrome. Cereb. Cortex 29, 3241–3252. https://doi.org/10.1093/cercor/bhy192.

Monnerie, H., Shashidhara, S., Le Roux, P.D., 2003. Effect of excess extracellular glutamate on dendrite growth from cerebral cortical neurons at 3 days in vitro: involvement of NMDA receptors. J. Neurosci. Res. 74, 688–700. https://doi.org/10.1002/jnr.10797.

Morello, M., Reiner, A., Sancesario, G., Karle, E.J., Bernardi, G., 1997. Ultrastructural study of nitric oxide synthase-containing striatal neurons and their relationship with parvalbumin-containing neurons in rats. Brain Res. 776, 30–39. https://doi.org/10.1016/s0006-8993(97)00997-9.

Podda, M.V., Grassi, C., 2014. New perspectives in cyclic nucleotide-mediated functionsin the CNS: the emerging role of cyclic nucleotide-gated(CNG) channels. Pflugers Arch. 466 (7), 1241–1257. https://doi.org/10.1007/s00424-013-1373-2 (Epub 2013 Oct 19).

Polito, M., Klarenbeek, J., Jalink, K., Paupardin-Tritsch, D., Vincent, P., Castro, L.R.V., 2013. The NO/cGMP pathway inhibits transient cAMP signals through the activation of PDE2 in striatal neurons. Front. Cell. Neurosci. 7, 211. https://doi.org/10.3389/fncel.2013.00211.

Sadek, M.S., Cachorro, E., El-Armouche, A., Kämmerer, S., 2020. Therapeutic implications for PDE2 and cGMP/cAMP mediated crosstalk in cardiovascular diseases. Int. J. Mol. Sci. 21, 7462. https://doi.org/10.3390/ijms21207462.

Salpietro, V., Perez-Dueñas, B., Nakashima, K., San Antonio-Arce, V., Manole, A., Efthymiou, S., Vandrovcova, J., Bettencourt, C., Mencacci, N.E., Klein, C., Kelly, M. P., Davies, C.H., Kimura, H., Macaya, A., Houlden, H., 2018. A homozygous loss-of-function mutation in PDE2A associated to early-onset hereditary chorea. Mov. Disord. 33, 482–488. https://doi.org/10.1002/mds.27286.

Sammut, S., Threlfell, S., West, A.R., 2010. Nitric oxide-soluble guanylyl cyclase signaling regulates corticostriatal transmission and short-term synaptic plasticity of striatal projection neurons recorded in vivo. Neuropharmacology 58, 624. https://doi.org/10.1016/j.neuropharm.2009.11.011.

Sancesario, G., Morello, M., Massa, R., Fusco, F.R., D'Angelo, V., Bernardi, G., 1996. NADPH-diaphorase neurons contacting the cerebrospinal fluid in the ventricles of rat brain. J. Cereb. Blood Flow Metab. 16, 517–522. https://doi.org/10.1097/00004647-199605000-00019.

Sancesario, G., Morello, M., Reiner, A., Giacomini, P., Massa, R., Schoen, S., Bernardi, G., 2000. Nitrergic neurons make synapses on dual-input dendritic spines of neurons in the cerebral cortex and the striatum of the rat: implication for a postsynaptic action of nitric oxide. Neuroscience 99, 627–642. https://doi.org/10.1016/s0306-4522(00)00227-x.

Sancesario, G., Giorgi, M., D'Angelo, V., Modica, A., Martorana, A., Morello, M., Bengtson, C.P., Bernardi, G., 2004. Down-regulation of nitrergic transmission in the rat striatum after chronic nigrostriatal deafferentation. Eur. J. Neurosci. 20, 989–1000. https://doi.org/10.1111/j.1460-9568.2004.03566.x.

Schiavi, S., Carbone, E., Melancia, F., di Masi, A., Jarjat, M., Brau, F., Cardarelli, S., Giorgi, M., Bardoni, B., Trezza, V., 2022. Phosphodiesterase 2A inhibition corrects the aberrant behavioral traits observed in genetic and environmental preclinical models of autism Spectrum disorder. Transl. Psychiatry 12, 1–10. https://doi.org/10.1038/s41398-022-01885-2.

Schulz, J.B., Matthews, R.T., Jenkins, B.G., Ferrante, R.J., Siwek, D., Henshaw, D.R., Cipolloni, P.B., Mecocci, P., Kowall, N.W., Rosen, B.R., 1995. Blockade of neuronal nitric oxide synthase protects against excitotoxicity in vivo. J. Neurosci. 15, 8419–8429. https://doi.org/10.1523/JNEUROSCI.15-12-08419.1995.

Shakur, Y., Holst, L.S., Landstrom, T.R., Movsesian, M., Degerman, E., Manganiello, V., 2001. Regulation and function of the cyclic nucleotide phosphodiesterase (PDE3) gene family. Prog. Nucleic Acid Res. Mol. Biol. 66, 241–277. https://doi.org/10.1016/s0079-6603(00)66031-2.

Skeberdis, V.A., Chevaleyre, V., Lau, C.G., Goldberg, J.H., Pettit, D.L., Suadicani, S.O., Lin, Y., Bennett, M.V.L., Yuste, R., Castillo, P.E., Zukin, R.S., 2006. Protein kinase a regulates calcium permeability of NMDA receptors. Nat. Neurosci. 9, 501–510. https://doi.org/10.1038/nn1664.

Stephenson, D.T., Coskran, T.M., Wilhelms, M.B., Adamowicz, W.O., O'Donnell, M.M., Muravnick, K.B., Menniti, F.S., Kleiman, R.J., Morton, D., 2009. Immunohistochemical localization of phosphodiesterase 2A in multiple mammalian species. J. Histochem. Cytochem. 57, 933–949. https://doi.org/10.1369/jhc.2009.953471.

Thompson, W.J., Appleman, M.M., 1971. Multiple cyclic nucleotide phosphodiesterase activities from rat brain. Biochemistry 10, 311–316.

Wang, X., Robinson, P.J., 1997. Cyclic GMP-dependent protein kinase and cellular signaling in the nervous system. J. Neurochem. 68, 443–456. https://doi.org/10.1046/j.1471-4159.1997.68020443.x.

Wang, X., Guo, J., Song, Y., Wang, Q., Hu, S., Gou, L., Gao, Y., 2018. Decreased number and expression of nNOS-positive interneurons in basolateral amygdala in two mouse models of autism. Front. Cell. Neurosci. 12, 251. https://doi.org/10.3389/fncel.2018.00251.

Weiss, S.W., Albers, D.S., Iadarola, M.J., Dawson, T.M., Dawson, V.L., Standaert, D.G., 1998. NMDAR1 glutamate receptor subunit isoforms in neostriatal, neocortical, and hippocampal nitric oxide synthase neurons. J. Neurosci. 18, 1725–1734. https://doi.org/10.1523/JNEUROSCI.18-05-01725.1998.

Weston, M.C., Degerman, E., Manganiello, V.C., Holst, L.S., 2003. cAMP/cGMP dual-specificity phosphodiesterases. Handb. Cell Signal. Elsevier 441–446.

Yousaf, H., Rehmat, S., Jameel, M., Ibrahim, R., Hashmi, S.N., Makhdoom, E.U.H., Iwaszkiewicz, J., Saadi, S.M., Tariq, M., Baig, S.M., Toft, M., Fatima, A., Iqbal, Z., 2023. A homozygous founder variant in PDE2A causes paroxysmal dyskinesia with intellectual disability. Clin. Genet. 104, 324–333. https://doi.org/10.1111/cge.14386.